Photonic crystal horn and array antennas

Andrew R. Weily,[1,2] Karu P. Esselle,[1] and Barry C. Sanders[2]
[1]*Department of Electronics, Macquarie University, Sydney, NSW 2109, Australia*
[2]*Department of Physics, Macquarie University, Sydney, NSW 2109, Australia*
(Received 10 February 2003; published 16 July 2003)

We introduce a defect-based horn antenna in a two-dimensional photonic crystal. Our numerical simulations demonstrate the efficient, highly directional nature of the antenna. It has a large operating bandwidth, low loss, and an operating frequency that is scalable to various regions of the electromagnetic spectrum. We also show that the photonic crystal horn antenna can be successfully used in an array configuration that uses a feed network made from photonic crystal waveguide circuits. The feed network and antennas have been integrated into a single photonic crystal device. This photonic crystal array antenna is shown to have high directivity and compact size while retaining the advantages of the photonic crystal horn antenna.

DOI: 10.1103/PhysRevE.68.016609 PACS number(s): 42.70.Qs, 42.82.Et, 41.20.Jb

I. INTRODUCTION

Photonic crystals (PCs) have introduced new possibilities in the design of radiating structures. PCs are dielectric structures that are periodic in one or more dimensions [1–3] and prevent the propagation of electromagnetic waves for a given band of frequencies, known as the photonic band gap (PBG). PCs were first used in the field of antennas to increase the radiation efficiency of planar devices [4]. Dipole antennas using two-dimensional and three-dimensional PC reflectors have also been implemented [5,6]. Resonators composed of defect structures in PCs have also been reported to create antennas with large directivities and high efficiencies. These resonator antennas have been realized using one-dimensional [7], two-dimensional [8], and three-dimensional [9] PCs. They have the advantage of being compact, but are limited in their operating bandwidth and still require metallic components. One widely used antenna technology that has good bandwidth is the metallic horn antenna. Composed of a hollow pipe of a particular cross-sectional shape, it is tapered to form a large opening. The type, direction, and amount of taper dictate the overall antenna performance.

Much of the fundamental theory of the horn antenna was developed during world war II [10] and further refined as time progressed. To address the problem of limited bandwidth in current PC based antennas, we introduce a different type of radiating structure that uses the concept of a horn antenna and the band gap of a PC. We call this structure the *photonic crystal horn antenna* (PCHA). It is made from a defect waveguide in a two-dimensional photonic crystal. The defect waveguide is then gradually tapered to a larger opening to form the radiating aperture of the antenna. A similar transition from a PC waveguide to free space has recently been reported [11]. The resulting radiation pattern and performance of this antenna are quite important in applications and we provide this analysis here.

The advantages of the PCHA are its large operating bandwidth, high directivity, low loss, and scalability. The bandwidth will be shown, under the proper design conditions, to be equal to that of a PC defect waveguide. The directivity may also be changed by varying the size of the radiating aperture. Since the PCHA is made completely from a dielectric material and contains no metal, the losses will be low, particularly at high frequencies where the skin effect loss of conductors tends to dominate. The operating frequency of the PCHA is also scalable to different regions of the electromagnetic spectrum, due to the scalability of Maxwell's equations. This property enables the PCHA to be used as an antenna at microwave and millimeter wave frequencies, as well as having applications as a source and/or receiver in optical systems.

Array antennas are used in applications that require very directive characteristics and extremely narrow radiation patterns, such as long distance communications. The PCHA introduced in this paper is also versatile enough to be used as the basic radiating element of an array antenna. We show how to use well-known PC components such as 90° bends and T junctions to build a *photonic crystal array antenna* (PCAA) which integrates the feed network and radiating elements into a single device. The PCAA retains most of the advantages of the PCHA, the main difference being that it has an increased directivity.

II. PHOTONIC CRYSTAL HORN ANTENNA

The configuration of the proposed two-dimensional PCHA is shown in Fig. 1. We have analyzed this antenna using a two-dimensional finite-difference time-domain

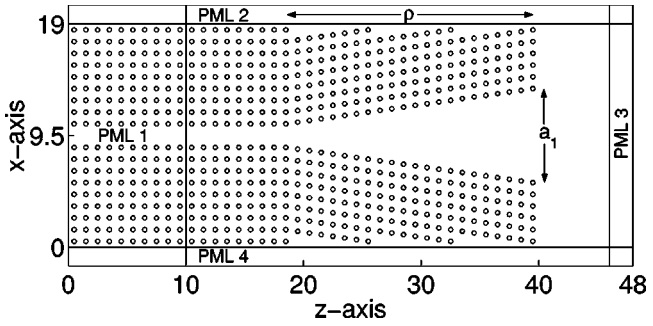

FIG. 1. Configuration of the two-dimensional photonic crystal horn antenna and computational domain used for its analysis. The units of each axis are given in lattice constants, a, to generalize the results presented. The excitation point is at $x=9.5a$ and $z=10a$.

(FDTD) method [12] and Berenger's perfectly matched layer (PML) [13]. The FDTD method is a direct solution of Maxwell's time-dependent curl equations. It replaces the spatial and temporal derivatives of these equations with finite-difference expressions, which leads to an algorithm that is accurate upto second-order. The approach gives explicit solutions to the time-domain electric- and magnetic-field intensities within the computational volume under analysis, thus avoiding the matrix inversions typically required by the solution of implicit equations. This gives the advantage that electrically large, complicated structures may be simulated, such as photonic crystals. Given its time-domain nature, solutions are broadband, and quantities may be easily transformed to the frequency domain using the discrete fourier transform.

Open regions and waveguide ports used when modeling antennas need to be terminated with absorbing boundary conditions (ABCs). ABCs absorb the outgoing electromagnetic waves while keeping unphysical reflections as low as possible to model the phenomena of a wave disappearing into free space or a mode traveling into a waveguide of infinite length. The PML has been shown to give low reflections in PC waveguides [14], so it is useful for terminating the feed section of the PCHA and the free space regions surrounding it. Figure 1 also shows the details of the FDTD computational domain used to analyze the antenna. The PC consists of circular dielectric rods in air positioned in a rectangular lattice, with a lattice constant a.

For the purpose of our analysis, the x axis corresponds the the vertical axis of Fig. 1, the z axis corresponds to the horizontal axis, and the y axis is parallel to the axis of the rods. We set the radius of the rods to $r=0.18a$ and the dielectric constant of the rods to 11.56. This PC structure has a TM_y band gap that extends in frequency from $\omega a/2\pi c=0.302$ to 0.443 [15]. For all FDTD simulations reported in this paper, the spatial discretization value used was $\Delta=a/25$ in both x and z directions. To terminate the waveguide feed section of the antenna a PML region that is $10a$ FDTD cells in length has been used (PML 1 in Fig. 1). The other boundaries used PML regions of ten FDTD cells. Figure 1 also shows the parameters that have been used to define the antenna. These parameters are the taper length ρ and the aperture width a_1.

To observe the effect of varying the taper length ρ and hence, the taper angle for the same size aperture width of $a_1=8a$, six different PCHA configurations with taper lengths of $\rho=6a$, $\rho=9a$, $\rho=12a$, $\rho=15a$, $\rho=18a$, and $\rho=21a$ have been analyzed. The spectrum of the pulse used to excite the antennas extended from $\omega a/2\pi c=0.330$ to 0.450. The reflection coefficient vs normalized frequency calculated using the FDTD method is shown in Fig. 2. From this figure, it is clear that increasing the taper length reduces the reflections at the input of the PCHA and extends the useful bandwidth of the device. For taper lengths greater than $\rho=15a$, the -10 dB bandwidth of the PCHA is 31%, which is equal to the operating bandwidth of the PC waveguide.

The far-field radiation pattern for the waveguide configuration with $\rho=21a$ and $a_1=8a$ have also been calculated using the FDTD method for the frequencies $\omega a/2\pi c=0.342$, $\omega a/2\pi c=0.374$, and $\omega a/2\pi c=0.405$. These frequencies have been chosen because they correspond to the lower, center, and upper operating frequencies of the PCHA array that will be examined in Sec. III. The radiation patterns for these frequencies are presented in Fig. 3, and are compared with the analytical formulas for the H-plane radiation pattern of a TE_{10} mode distribution aperture on a metallic ground plane, where the TE_{10} mode corresponds to that of a rectangular metallic waveguide [16]. The simplified analytical expression for these radiation patterns is

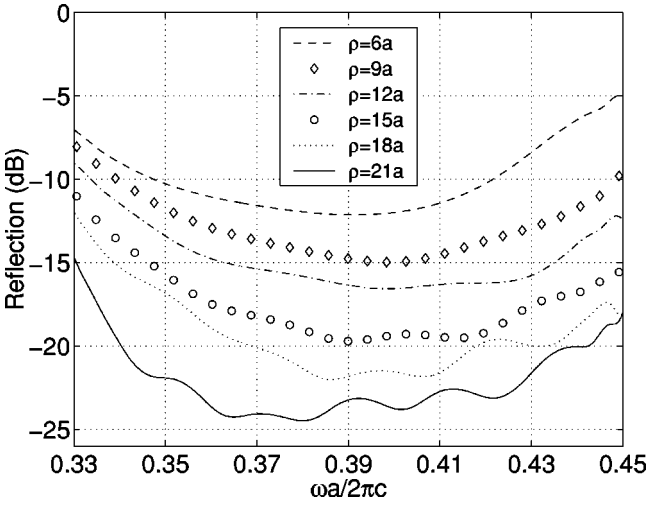

FIG. 2. Computed reflection coefficient versus normalized frequency for six photonic crystal horn antennas with different taper lengths. For each antenna the aperture width used is $a_1=8a$.

$$E_y^{\mathrm{ff}}=-\frac{\pi}{2}C\cos\theta\frac{\cos X}{X^2-(\pi/2)^2}, \tag{1}$$

$$X=\frac{\pi a_1}{\lambda}\sin\theta, \tag{2}$$

with C a normalizing constant and θ is the polar angle measured from the z axis.

The definition of a_1 given in Fig. 1 is from center to center of the rods that form the mouth of the PCHA. A more accurate estimate is from the inner edge of the rods, which gives $a_1=8a-2r=7.64a$. The patterns presented in Fig. 3 give reasonable agreement with the analytical expressions of Eq. (1), particularly for the main lobe, and show the directive nature of the PCHA at each frequency. The half-power beamwidths (HPBW) W_{HP} computed using FDTD are 28.6°, 24.7°, and 22.0° for the respective frequencies $\omega a/2\pi c=0.342$, 0.374, and 0.405. The first null beamwidths (FNBW) W_{FN} computed using FDTD are 70°, 62°, and 54° for the respective frequencies $\omega a/2\pi c=0.342$, 0.374, and 0.405. These values can also be estimated with reasonable accuracy using the H-plane formulas for a TE_{10} mode distribution aperture on a metallic ground plane [16]. These formulas are based on an analytical solution and may be calculated as follows:

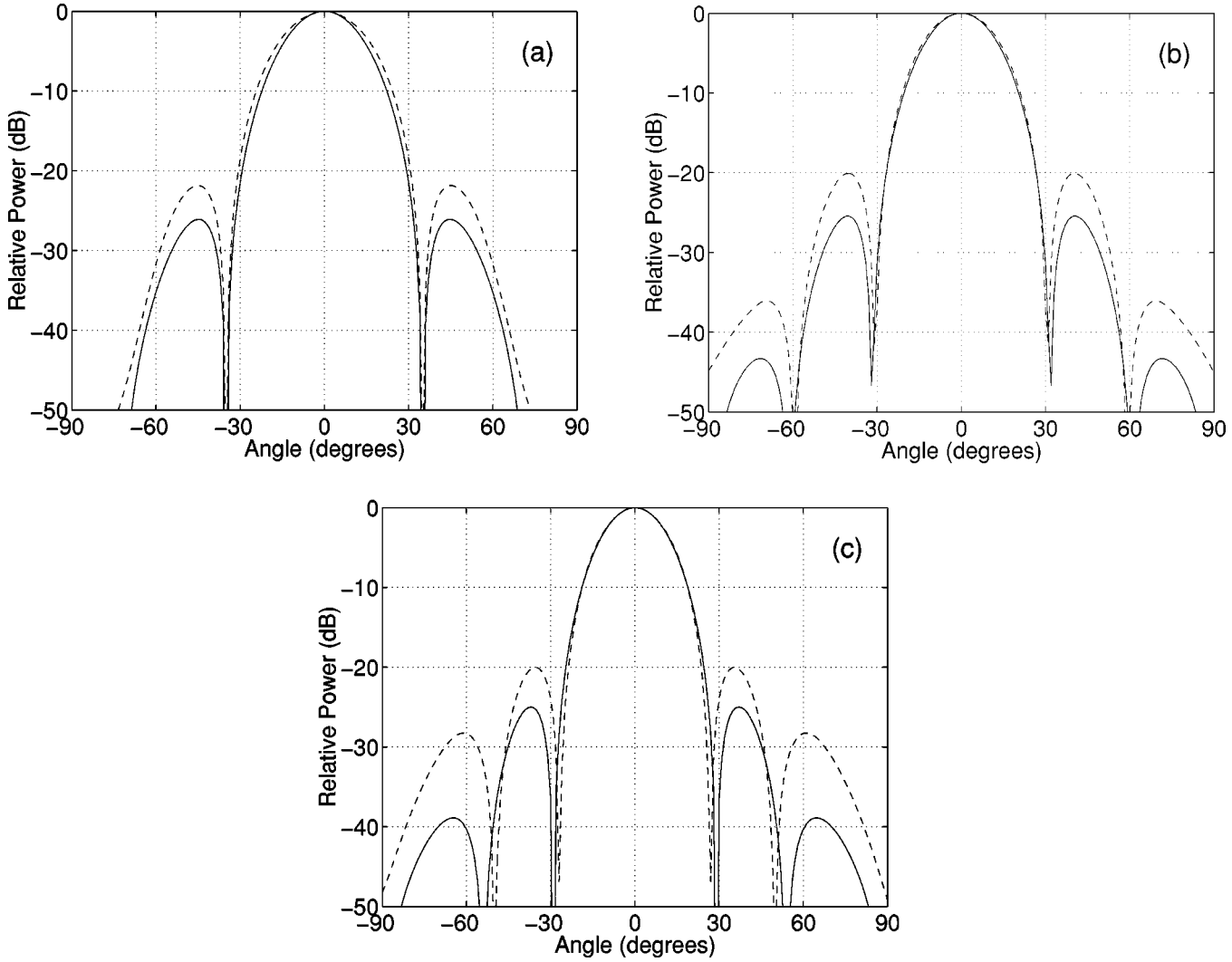

FIG. 3. Computed radiation pattern for the photonic crystal horn antenna at (a) $\omega a/2\pi c=0.342$, (b) $\omega a/2\pi c=0.374$, and (c) $\omega a/2\pi c=0.405$. The taper length is $\rho=21a$ and the aperture width is $a_1=8a$. The solid line corresponds to theory and the dashed line corresponds to FDTD.

$$W_{\mathrm{HP}}=\frac{68.8}{a_1/\lambda} \quad \text{degrees,} \tag{3}$$

$$W_{\mathrm{FN}}=\frac{171.9}{a_1/\lambda} \quad \text{degrees.} \tag{4}$$

Using a value of $a_1=7.64a$ in Eq. (3) gives the HPBWs of 26.3°, 24.1°, and 22.2° for the respective frequencies $\omega a/2\pi c=0.342$, 0.374, and 0.405. From Eq. (4), the FNBWs are 65.7°, 60.2°, and 55.5° for the respective frequencies $\omega a/2\pi c=0.342$, 0.374, and 0.405. From Ref. [16], the first sidelobe level is given as 23 dB below the major lobe, which compares well with the FDTD range of 20−21 dB. Using these simple formulas, we can efficiently obtain an accurate estimate of the PCHA's radiation performance.

To give more insight into the operation of the PCHA, a linear scale field plot is presented in Fig. 4. This plot has been calculated for the frequency $\omega a/2\pi c=0.392$ by taking the discrete fourier transform of the time-domain fields. The

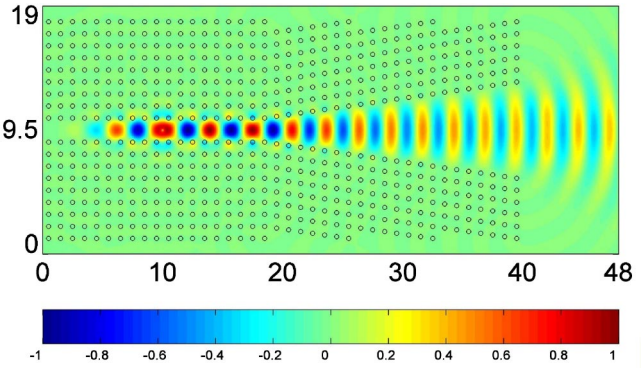

FIG. 4. (Color online) E_y field of the photonic crystal horn antenna at $\omega a/2\pi c=0.392$, plotted in linear scale. The fields have been normalized so that the maximum value is 1 and the minimum value is −1.

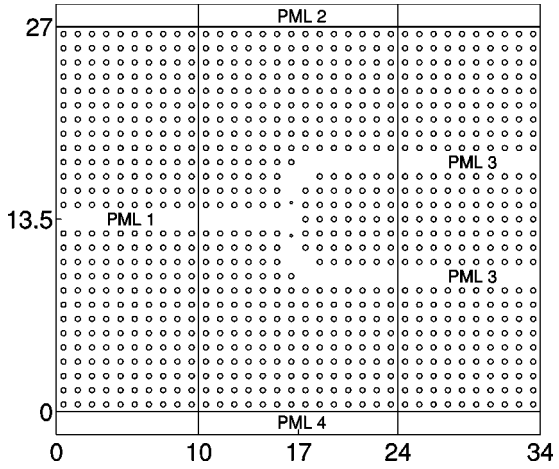

FIG. 5. Configuration of the photonic crystal *T* junction and two 90° bends. The excitation point is at $x=13.5a$ and $z=10a$. (Axes and notation as for Fig. 1.)

plot clearly shows the profile of the propagating mode in the PC defect waveguide and its transition to a spherical wave in free space, via the tapered section of the PCHA.

III. PHOTONIC CRYSTAL ARRAY ANTENNA

In many applications, such as long distance communications, the directivity that can be obtained with a single antenna is not high enough. These situations require an antenna with a large electrical size to increase the directivity and sharpen the radiation pattern. This may be achieved by using an array of antennas that focuses the electromagnetic energy in a particular direction through the action of constructive interference. The radiating elements used in the array are usually identical. Further, it is possible to shape the radiation pattern of the array by varying its parameters. These parameters are the number of elements used and their geometrical configuration, the element spacing, the excitation amplitude and phase of each element, and the radiation pattern of each

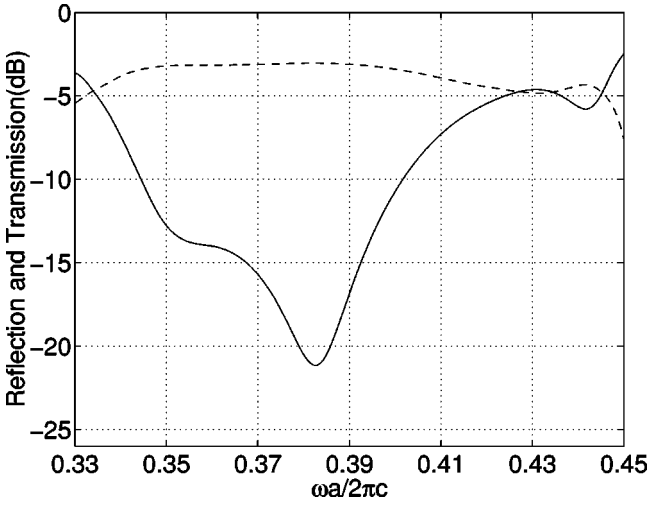

FIG. 6. Computed transmission (dashed line) and reflection (solid line) coefficients vs normalized frequency for the photonic crystal *T* junction and two 90° bends.

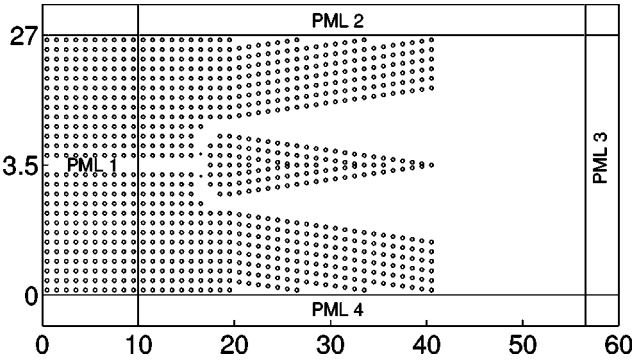

FIG. 7. Configuration of the two-element photonic crystal array antenna and computational domain used for its analysis. Each antenna has an aperture width of $a_1=8a$ and a taper length of $\rho=21a$. The excitation point is at $x=13.5a$ and $z=10a$. (Axes and notation as for Fig. 1.)

element. Here, we analyze an array that is formed by placing the individual elements in a line. This is the simplest formation available and is known as a linear array. An approximate radiation pattern may be calculated by multiplying the radiation pattern of an individual antenna element with the array factor (AF) F_{A} of the array [16], as follows:

$$E^{\mathrm{ff}}_{\mathrm{array}}=[E^{\mathrm{ff}}_{\mathrm{element}}][F_{\mathrm{A}}], \tag{5}$$

where the AF depends on the array configuration, element spacing, excitation amplitude, and phase for each array element. For the linear array, the normalized AF may be expressed as

$$F_{\mathrm{A}}=\frac{1}{N}\left[\frac{\sin(N\psi/2)}{\sin(\psi/2)}\right], \tag{6}$$

where

$$\psi=\frac{2\pi d}{\lambda}\sin\theta, \tag{7}$$

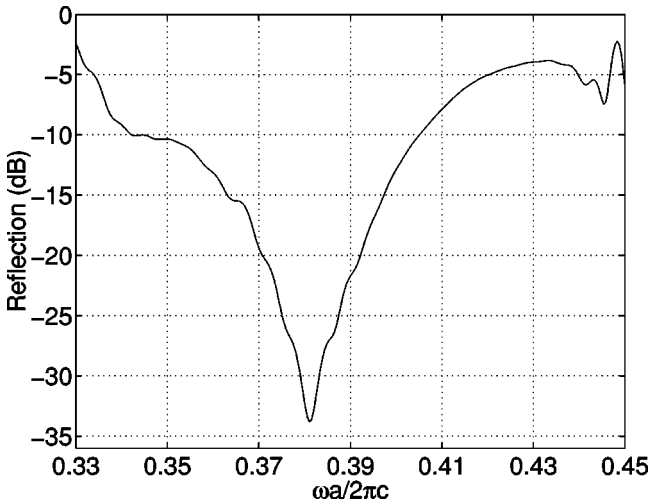

FIG. 8. Computed reflection coefficient vs normalized frequency for the two-element photonic crystal array antenna.

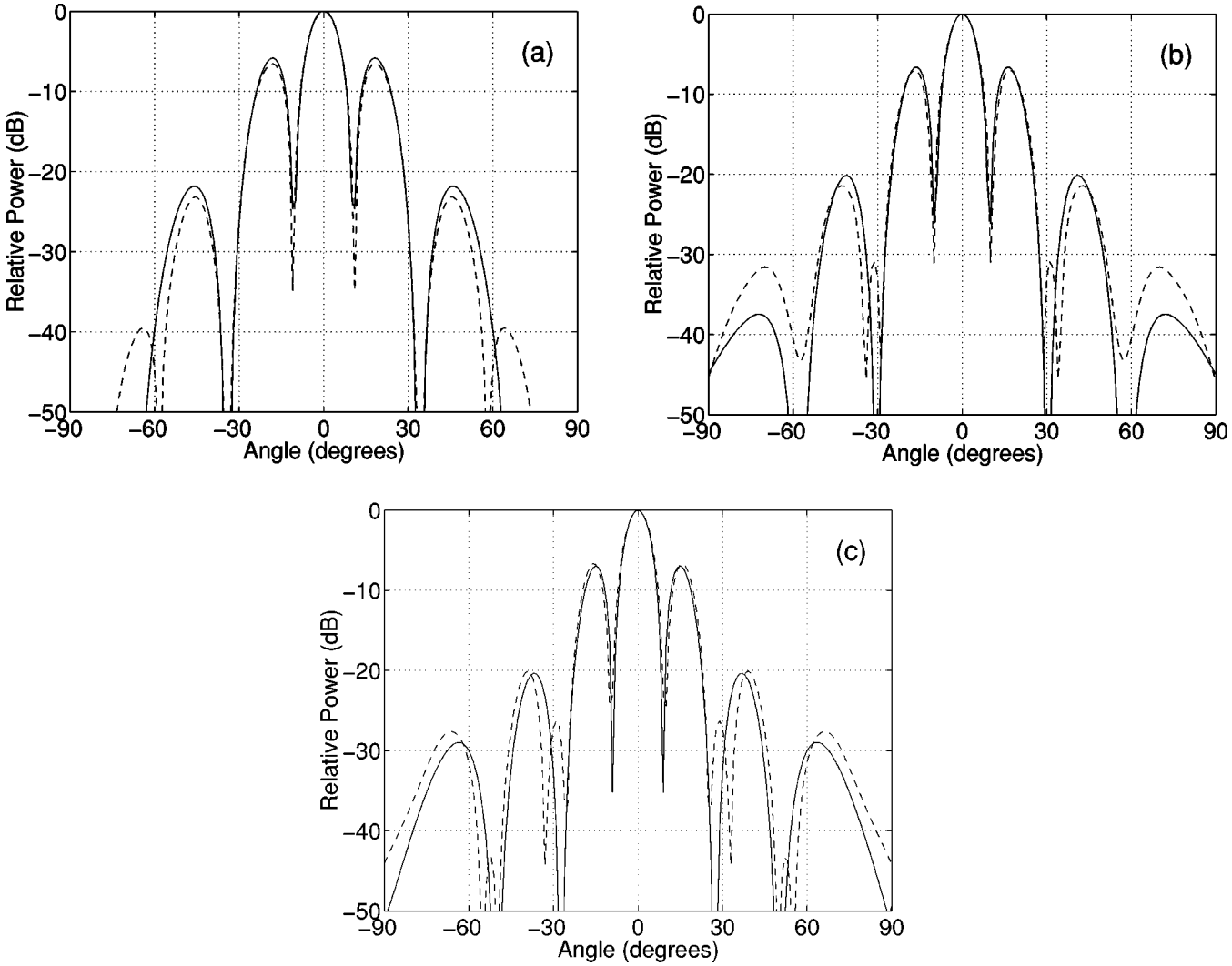

FIG. 9. Computed radiation patterns for the two-element photonic crystal array antenna at (a) $\omega a/2\pi c=0.342$, (b) $\omega a/2\pi c=0.374$, and (c) $\omega a/2\pi c=0.405$. The solid line corresponds to array theory and the dashed line corresponds to FDTD.

with N equal to the number of array elements and d equal to the separation between two adjacent elements.

To create a PCAA, we require a feed network to distribute the input power to each element of the array. This can be accomplished by using a PC T junction [17] plus two 90° bends [15], which is depicted in Fig. 5. Adding extra rods between the input and output waveguides increases the transmission of the T junction [17]. Beyond this, we have observed that by changing the separation of these extra rods, it is possible to tune the frequency of maximum transmission. The radius of the extra rods used in our design was $r_t=0.08a$ and the separation between the rods was $2.32a$. Computed transmission and reflection coefficients versus normalized frequency for the T junction are given in Fig. 6. This figure shows that the maximum transmission and minimum reflection occurs at $\omega a/2\pi c=0.383$, with -3 dB or 50% of the input power being transmitted into each output waveguide. The bandwidth of the T junction is also good, with more than 45% of the input power being transmitted into each output waveguide for $\omega a/2\pi c=0.344$ to 0.402 or a bandwidth of 15.5%.

The feed network just described has been used to design a two-element linear array, as shown in Fig. 7. This array uses the PCHA introduced earlier in this paper as its basic radiating element. Figure 7 also gives details on the FDTD computation domain used to analyze the array such as the size of the domain in terms of lattice constants and the location of the PML boundaries. Each PCHA has an aperture width of $a_1=8a$ and a taper length of $\rho=21a$. Using the computational domain of Fig. 7, the reflection coefficient for the array antenna has been computed and is plotted in Fig. 8. This figure shows the operating region of the array is $\omega a/2\pi c=0.342$ to 0.405 and has an operating bandwidth of 17%. The far-field radiation pattern for the two-element array has also been calculated using FDTD at the frequencies $\omega a/2\pi c=0.342$, $\omega a/2\pi c=0.374$, and $\omega a/2\pi c=0.405$.

A comparison between the FDTD computed radiation patterns and those calculated from the array theory of Eqs. (5)–(7) is presented in Fig. 9. The individual element radiation patterns used in the array theory calculation [$E^{\mathrm{ff}}_{\mathrm{element}}$ in Eq. (5)] are the FDTD computed values shown in Fig. 3. There is good agreement between array theory and FDTD in Fig. 9,

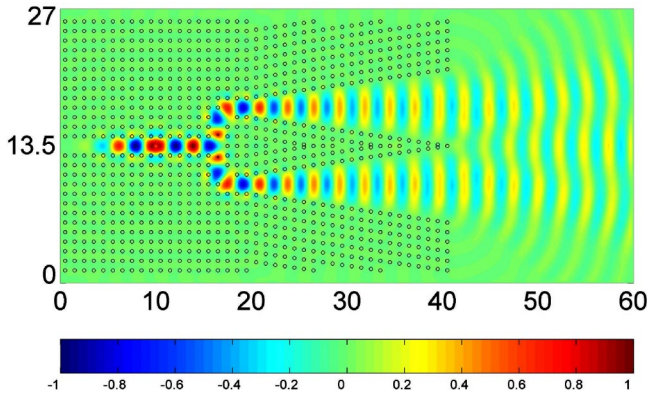

FIG. 10. (Color online) E_y field of the two-element photonic crystal array antenna at $\omega a/2\pi c = 0.392$, plotted in linear scale. The fields have been normalized so that the maximum value is 1 and the minimum value is -1.

with a small discrepancy in the sidelobes caused by the omission of the mutual coupling between array elements in the array theory calculation. This result leads us to conclude that array theory applies equally well to PCAAs as it does to standard array antennas, thus providing a simple approach for accurately predicting PCAA radiation performance. It also indicates that there is no significant mutual coupling between the two PCHAs even though they are located next to each other.

The HPBWs for the PCAA are 10°, 8.9°, and 8.2° for the frequencies $\omega a/2\pi c = 0.342$, 0.374, and 0.405, respectively. The FNBWs are 21°, 20°, and 18° for the respective frequencies $\omega a/2\pi c = 0.342$, 0.374, and 0.405, while the first sidelobe level is 6.5 dB below the major lobe. Comparing Fig. 9 to Fig. 3, it is apparent that more sidelobes and nulls appear in the radiation pattern of the array due to constructive and destructive interference effects between the two array elements. To demonstrate the operation of the array antenna a field plot for $\omega a/2\pi c = 0.392$ is given in Fig. 10. This plot shows the input signal being split into two parts by the *T* junction, followed by two 90° bends that direct the signal to the PCHAs. The output of the PCHAs then generates an interference pattern that creates a highly directional main beam in the free space region.

IV. CONCLUSION

We have demonstrated a different type of radiating device, the photonic crystal horn antenna (PCHA), which is made from a tapered defect waveguide in a two-dimensional PC. For gradual taper values, highly efficient transmission from the PC waveguide to free space is obtained over the entire bandwidth of the waveguide. This is equal to a 31% bandwidth. The PCHA also has the added advantages of low loss and a scalable operating frequency. Far-field radiation patterns have been computed for the PCHA and showed the directional nature of the structure. Simple formulas have been presented that accurately predict the PCHA far-field patterns and parameters such as HPBW and FNBW.

A photonic crystal array antenna (PCAA) composed of two PCHAs has also been presented. The array feed network was constructed from a PC *T* junction and two 90° PC waveguide bends. The feed network and PCHAs were integrated into a single device. The array was demonstrated theoretically to give low reflections over a 17% bandwidth and has a highly directional radiation pattern. Array theory has been used to accurately predict the PCAA far-field radiation pattern from the radiation pattern of a single PCHA. Mutual coupling between the two PCHAs was found to be insignificant even though they are located next to each other. The concepts of the PCHA and PCAA given here are expected to have a wide range of useful applications in the future at microwave, millimeter, and optical frequencies.

ACKNOWLEDGMENT

This research was funded by an Australian Research Council Discovery Grant.

[1] J.D. Joannopoulos, R.D. Meade, and J.N. Winn, *Photonic Crystals: Molding the Flow of Light* (Princeton University Press, Princeton, NJ, 1995).
[2] E. Yablonovitch, Phys. Rev. Lett. **58**, 2059 (1987).
[3] S. John, Phys. Rev. Lett. **58**, 2486 (1987).
[4] E.R. Brown, C.D. Parker, and E. Yablonovitch, J. Opt. Soc. Am. B **10**, 404 (1993).
[5] M.P. Kesler, J.G. Maloney, and B.L. Shirley, Microwave Opt. Technol. Lett. **11**, 169 (1996).
[6] G.S. Smith, M.P. Kesler, and J.G. Maloney, Microwave Opt. Technol. Lett. **21**, 191 (1999).
[7] C. Serier, C. Cheype, R. Chantalat, M. Thévenot, T. Monédière, A. Reinex, and B. Jecko, Microwave Opt. Technol. Lett. **29**, 312 (2001).
[8] C. Cheype, C. Serier, M. Thévenot, T. Monédière, A. Reinex, and B. Jecko, IEEE Trans. Antennas Propag. **50**, 1285 (2002).
[9] R. Biswas, E. Ozbay, B. Temelkuran, M. Bayindir, M.M. Sigalas, and K.M. Ho, J. Opt. Soc. Am. B **11**, 1684 (2001).
[10] A.W. Love, *Electromagnetic Horn Antennas* (IEEE Press, New York, 1976).
[11] E. Moreno, D. Erni, and C. Hafner, Phys. Rev. E **66**, 036618 (2002).
[12] A. Taflove and S.C. Hagness, *Computational Electrodynamics: The Finite-Difference Time-Domain Method*, 2nd ed. (Artech House, Boston, 2000).
[13] J.P. Berenger, J. Comput. Phys. **114**, 185 (1994).
[14] M. Koshiba, Y. Tsuji, and S. Sasaki, IEEE Microw. Wirel. Compon. Lett. **11**, 152 (2001).
[15] A. Mekis, J.C. Chen, I. Kurland, S. Fan, P.R. Villeneuve, and J.D. Joannopoulos, Phys. Rev. Lett. **77**, 3787 (1996).
[16] C.A. Balanis, *Antenna Theory: Analysis and Design*, 2nd ed. (Wiley, New York, 1996).
[17] S. Fan, S.G. Johnson, J.D. Joannopoulos, C. Manolatou, and H.A. Haus, J. Opt. Soc. Am. B **18**, 162 (2001).